Inteligencia Artificial 28(75), 170-185
doi: 10.4114/intartif.vol28iss75pp170-185

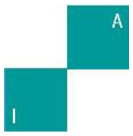

INTELIGENCIA ARTIFICIAL

http://journal.iberamia.org/

Recurrence Quantification Analysis (RQA) Features vs. Traditional EEG Features for Alzheimer's Disease Diagnosis

Mennato-Allah Talaat Mostafa [1], Medhat Awadalla LastName[2], Lamiaa Abdel-Hamid [1]

[1] Electronics and Communication Department, Faculty of Engineering, Misr International University, Cairo, Egypt
[2] Department of Computers and Systems, Faculty of Engineering, Helwan University, Cairo, Egypt

Abstract - Alzheimer's disease (AD) is a neurological disorder that causes memory decline and loss of cognitive abilities. AD directly impacts the brain activity of affected individuals, which can be reflected in electroencephalogram (EEG) signals. Previous studies have typically relied on statistical, spectral, and wavelet features in order detect AD using EEG signals. Recurrence Quantification Analysis (RQA) is a non-linear technique that has been successfully used to analyze EEG signals in several other domains including emotion recognition and autism detection. However, RQA features have not yet been fully investigated for AD diagnosis. The aim of this work is to thoroughly investigate the usefulness of RQA features for AD diagnosis. Fifteen RQA features were computed along with statistical measures, Hjorth parameters, and relative power in order to compare the performance of the RQA features to other commonly utilized EEG features. All features were computed from the different brain regions. Experimental results indicated that RQA features outperformed all other feature groups regardless of the considered brain region. RQA features achieved accuracies ranging from 89.6% to 98.2% using a support machine vector (SVM) classifier with leave-one-subject-out (LOSO) cross-validation. These results are between 25% to 40% higher than the three other considered feature groups. Feature ranking was performed to find the most relevant RQA features, identifying seven of the fifteen computed RQA features. This work sheds light on the potential of RQA features for reliable AD diagnosis and paves the way for their integration in computer-aided AD diagnostic tools using EEG signals.

Keywords: Alzheimer's disease (AD), recurrence quantification analysis (RQA), electroencephalogram (EEG), computer-aided-diagnosis, machine learning.

1 Introduction

Alzheimer's disease (AD) is an irreversible neurodegenerative disorder that causes progressive loss in memory and cognitive abilities. According to the World Health Organization (WHO), more than 55 million people are affected by AD worldwide [1]. AD symptoms include memory loss, difficulty in reasoning and decision-making, loss of coordination, inability to complete basic daily tasks such as dressing or eating, increased anxiety or aggression, mood swings, personality changes, difficulty with language and shortened attention span. More severe symptoms include hallucinations, paranoia, seizures, loss of bladder control, lack of communication, severe weight loss, and no awareness of surroundings or recent experiences [2]. Due to the major behavioural, emotional, and cognitive changes related to the disease, AD not only has devastating effect on patients but also on their care givers and families. There is currently no medication for the compete cure of AD [3]. However, available treatments can slow down disease progression and help manage disease symptoms more effectively.

Electroencephalogram (EEG) is a non-invasive technique that measures the electrical activity of the brain signals. EEG has several merits including low cost, availability, portability, and high temporal resolution. EEG can thus efficiently capture the brain dynamics associated with neurological disorders [6]. Several studies have shown that AD leads to several changes in the characteristics of EEG signals making them a good candidate for reliable automated AD diagnosis [7]. The international 10/20 system is a standardized method for EEG electrode placement for recording brain activity. This standard system ensures the coverage of all major regions of the brain in order to fully capture the electrical activity associated with various functions across the main brain regions [8].

ISSN: 1137-3601 (print), 1988-3064 (on-line)

The human brain is generally divided into four main lobes: frontal, parietal, occipital, and temporal. Each brain region is responsible for different cognitive functions [9], [10]. The frontal lobe is responsible for higher cognitive functions like problem-solving, decision-making, and voluntary behaviour. The parietal lobe integrates sensory information for orientation and movement. The occipital lobe is primarily involved in visual processing, whereas the temporal lobe handles auditory processing, memorizing, forming words, and language development. Each EEG channel is annotated with a letter and a number to identify the specific brain region and hemisphere location: frontal (F), temporal (T), parietal (P), and occipital (O). Additionally, electrodes placed over the central sulcus, which is located between the frontal and parietal lobes, are denoted by the letter (C) [11]. Central electrodes measure EEG activity from the combined frontal and temporal lobes. Figure 1 shows the main brain regions and the international 10/20 system. At its earlies stages, AD typically affects the parts of the brain responsible for memory, including the entorhinal cortex and the hippocampus located in the temporal lobe. As the disease progresses, it affects the patient's reasoning, language, social behaviour, vision, and orientation leading to widespread impairment across the different brain regions [12].

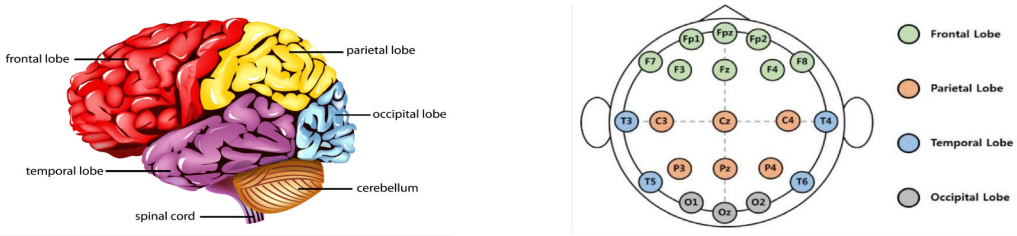

Figure 1. 10-20 Main brain regions [10] and EEG electrode placement system [8].

AD has been shown to cause alterations in both the complexity and power spectrum of patients' EEG signals [13] [14]. EEG complexity refers to the variability and richness of the signal over time. In healthy patients, EEG signals exhibit complex dynamic patterns due to the brain's adaptability and cognitive functioning. In AD patients, there is a marked reduction in the complexity of EEG signals that can be linked to the decline in their cognitive abilities. Additionally, there is often a shift in the power spectrum of the EEG signal of AD patients. Specifically, there is an increase in low-frequency activity and a decrease in higher-frequency activity. Based in these changes in EEG patterns, various machine learning methods have been applied to distinguish AD patients from healthy subjects (HS) using different types of EEG features. Recurrence quantification analysis (RQA) is a non-linear method for EEG analysis. RQA features have been previously shown to give superior performance in several EEG-based studies such as emotion detection [15], autism diagnosis [16], and epilepsy identification [17]. Despite their potential to thoroughly capture changes in the characteristics of EEG signals [18], [19], RQA features have been scarcely implemented in literature for AD diagnosis.

In this work, RQA features are compared to three widely used EEG feature groups (statistical – Hjorth – relative power) for AD diagnosis. Specifically, fifteen different RQA features are computed to fully capture changes in the EEG signal due to AD progression. All features were computed from the different brain regions in order to compare their relevance for AD detection. Experimental results showed that the RQA features achieved significantly better performance than all the other feature groups regardless of the brain region considered for feature extraction. Furthermore, the proposed method outperformed several other approaches from literature using the same dataset, with the added advantage of relying on a limited number of EEG channels for feature extraction.

2 Related Works

Machine learning approaches have been widely implemented in literature for the diagnosis of AD from EEG signals. Several classifiers were considered including support machine vector (SVM), k-nearest neighbour (KNN), linear discriminant analysis (LDA), decision trees (DT), and random forest (RF). Deep learning-based approaches have also been investigated for AD diagnosis from EEG signals. However, deep learning-based methods are still in their early stages due to the limitations in the size of the available EEG datasets.

Generally, EEG features can be divided into time, spectral, transform, and deep features [20], [21]. Time-domain features include simple statistical features such as mean, variance, skewness, and entropy-based features. In addition, more sophisticated complexity features can be extracted from the EEG signal's time domain such as Hjorth parameters, fractal dimensions (FD), and RQA features. Spectral features are computed from the frequency representation of the EEG signal such as the Fast Fourier Transform (FFT). Frequency-domain features include

the power spectral density (PSD) as well as the relative powers of different EEG frequency bands. Transform-based features are extracted from time-frequency representations of the signal, most commonly the wavelet transform (WT). WT works by applying a series of successive high and low frequency filters which are used to decompose the EEG signal into the delta, theta, alpha, beta, and gamma subbands. Wavelet features refer to statistical or complexity measures computed from the wavelet decomposed subbands. Deep features refer to features automatically extracted using deep networks. Inputs to the deep networks can be the raw EEG signals, traditional features, or images representations obtained from the EEG signal's Fourier Transform (spectrograms) or Wavelet Transform (scalograms).

Table 1 summarizes several AD diagnosis approaches from literature indicating the dataset, EEG channels, implemented features, classifier, cross-validation approach, and accuracy. Most AD diagnosis methods considered EEG features computed from the entire brain region. Among the differences between them is that some consider all the recorded EEG channels from the different brain regions, whereas others performed some sort of analysis to select the most relevant channels. Limiting the number of EEG channels has the advantage of reduced computational complexity as well as the potential to use simpler EEG headsets, i.e. portable EEG handsets. As for the computed EEG features, AD detection methods typically relied on a combination of simple statistical features along with spectral features, most commonly relative power. Some works also investigated complex features, such as Hjorth parameters showing that they significantly improved results [22]. However, few works implemented RQA features for AD diagnosis. An early work by Timothy et al. [18] considered RQA and cross RQA for discriminating between early AD and HS. However, they computed only a single RQA feature which is the recurrence rate (RR). Their results barely reached 80% accuracy considering leave-one-subject-out (LOSO) cross validation (CV). In a previous work for emotion detection, Mona et al. [15] computed eleven RQA features from six EEG channels (frontal and central) to classify emotional valence and arousal. Their approach resulted in superior performance achieving accuracies that were up to 20% higher than various EEG feature types. RQA features have, however, not yet been fully explored for AD diagnosis.

Table 1. Summary of AD detection methods in literature.

Paper	Year	Dataset	EEG Channels	Features	Classifier	CV	Accuracy
Timothy et al. [18]	2017	18 AD 18 HS	FCPOT (excluding Fp1, Fp2)	RQA (RR)	LDA	LOSO	72.20%
				CRQA (RR)			80.60%
Tzimourta et al. [23]	2019	14 AD 10 HS	FCPOT (11 channels)	Spatial Spectral	RF	10-fold	91.80%
Miltiadous et al. [24]	2021	10 AD 8 HS	FCPOT	Spatial Spectral	DT	LOSO	78.50%
					RF	10-fold	99.1%
Safi and Safi [22]	2021	51 AD 35 HS	FCPOT	Wavelet	SVM	LOSO	81.00%
						Monte Carlo	97.64%
Miltiadous et al. [25]	2023	36 AD 29 HS	FCPOT	Spectral	RF	LOSO	77.00%
Zheng et al. [26]	2023	36 AD 29 HS	FCPOT	Spatial Spectral	RF	LOSO	95.86%
Zhou et al. [27]	2023	36 AD 29 HS	FCPOT	EEG-Net		5-fold	93.30%
Amer and Belhaouari [28]	2024	10 AD 8 HS	FPOT (6 channels)	GoogLeNet		--	95.90%

In the present study, 15 RQA features were computed to investigate their usefulness for AD diagnosis. Additionally, their performance was compared to the widely implemented statistical, Hjorth, and relative power features. All features were computed from the different brain regions to identify the feature group and brain region most relevant for AD diagnosis. Feature ranking was also performed to identify the most relevant RQA features for AD diagnosis. Finally, the proposed method was compared to various other methods from literature considering the same dataset.

3 Methods

In the present study, the main objective is to investigate the usefulness of RQA features for AD diagnosis and compare their performance to several widely implemented features which are Hjorth, statistical, and relative power. Figure 2 provides an overview of the experimental workflow considered in this work.

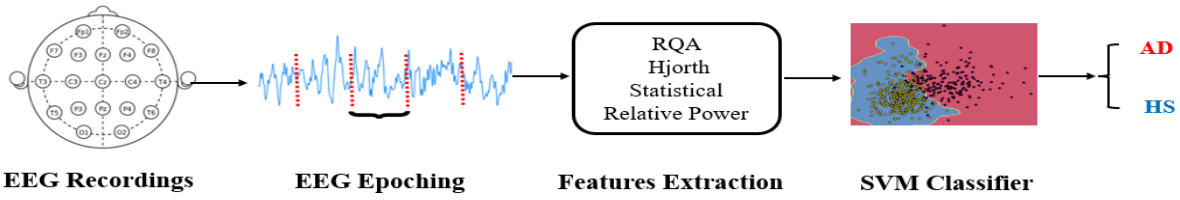

Figure 2. Experimental Workflow.

3.1 Feature Extraction

3.1.1 Recurrence Quantification Analysis (RQA) Features

Recurrence is a fundamental principal in many dynamical systems through which system characteristics can be interpreted. Eckmann et al. [29] introduced a graphical representation to capture recurrence in complex dynamic systems known as the recurrence plot (RP). RP is an m-dimensional phase space that could be explored through a two-dimensional *NxN* square matrix *R*. RP represents the number of instances at which state x_i recur, or in other words, the recurrence of a state at time *i* at a different time *j* [30]. Such recurrence is represented with dots on the *R* matrix (both *i* and *j* axes being time), where a dot is positioned at *(i,j)* each time x_i can proximate x_i [29]. The time series x_i is then established by the means of "time delays" embedding dimension method as follows:

$$x_i = (u_i + u_{i+\tau}, \ldots\ldots, + u_{i+\tau(m-1)}) \quad (1)$$

where m is the embedding dimension and τ is the time delay.

The recurrence of states is then defined as:

$$R_{i,j}^{m,\varepsilon_i} = \Theta\left(\varepsilon - \|x_i - x_j\|\right), x_i \in R^m, i, j = 1, \ldots N \quad (2)$$

where N is the number of considered sates, ε is a threshold distance, $\|\cdot\|$ is the norm and $\Theta(\cdot)$ is the Heaviside function. For the Heaviside function, $\Theta(x)=0$ if $x<0$ and $\Theta(x)=1$ otherwise [31].

The RP is obtained by plotting the recurrence matrix from Eq. (2). For the coordinates *(i,j),* a black dot is plotted if $R_{i,j}=1$, i.e. in the recurrent state and a white dot is plotted if $R_{i,j}=0$. Recurrent states tend to form different lines and structures that reflect the underlying dynamics of the signal. Diagonal, vertical, and horizontal lines can be easily observed within the RP. These represent different aspects of the dynamics of a system, such as its stability, periodicity, and predictability. Diagonal lines are formed when the system's state follows similar trajectories at different times. Longer black diagonal lines indicate that the system behaves similarly for extended periods suggesting regularity and predictability. Vertical and horizontal lines reflect how long a system stays in the same state for multiple time steps. Short vertical or horizontal lines thus indicate dynamic and changing behavior. An example of a RP of an EEG recording is shown in Figure 3.

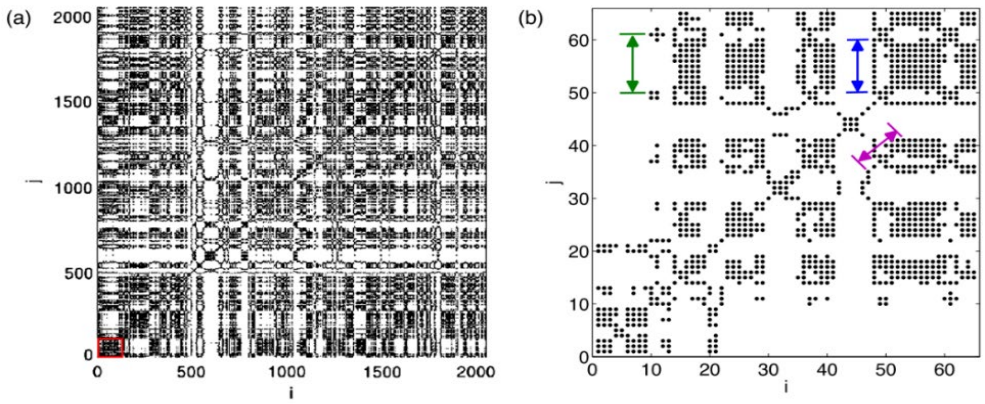

Figure 3. (a) Example for an EEG RP – (b) enlarged area for the lower left corner of the original plot [32].

Although RPs offer a comprehensive qualitative evaluation for EEG signals, their visual inspection is an extremely complicated process. Several publications have introduced different measures to quantify RP structures under the name of RQA features. In the present work, fifteen RQA features are investigated in order to thoroughly capture the complexity of the EEG signals [31-35]. The details of the implemented features can be summarized as follows:

1. **Recurrence Rate (RR):** measures the probability that the studied process will recur through counting the black dots in the RP.

$$RR = \frac{1}{N^2}\sum_{i,j=1}^{N} R_{i,j} \tag{3}$$

2. **Determinism (DET):** is the ratio between recurrence points forming diagonal lines to all recurrent points. DET reflects the predictability and regularity in the system.

$$DET = \frac{\sum_{l=l_{min}}^{N} lP(l)}{\sum_{i,j}^{N} lP(l)} \tag{4}$$

where ***P(l)*** is the probability distribution of the lengths of the diagonal lines and l_{min} is the least considered line length.

3. **RATIO:** is defined as the ratio between DET and RR. It quantifies the balance between the deterministic structure and the overall recurrence rate observed in the signal.

$$RATIO = \frac{DET}{RR} \tag{5}$$

4. **Average Diagonal Length (L):** is the average length of diagonal lines, representing the predictability of the system.

$$L = \frac{\sum_{l=l_{min}}^{N} lP(l)}{\sum_{l=l_{min}}^{N} P(l)} \tag{6}$$

5. **Length of longest diagonal (Lmax):** measures the length of the longest line in the RP, representing the longest time the system remains in a specific state.

$$L_{max} = \max\left(\{l_i\}_{i=1}^{N_l}\right) \tag{7}$$

where $N_l = \sum_{l \geq l_{min}} P(l)$ is the total number of diagonal lines.

6. **Divergence (DIV):** is the inverse of $L_{max,}$ measuring how quickly two initially close trajectories in the state space become distant from each other.

$$DIV = \frac{1}{L_{max}} \tag{8}$$

7. **Entropy (ENT):** is the probability that a diagonal has an exact length *l*. ENT measures the degree of randomness thus assessing the complexity and predictability of the system.

$$ENT = \sum_{l=l_{min}}^{N} p(l) \ln p(l) \tag{9}$$

8. **Laminarity (LAM):** is the ratio between the recurrent points forming the vertical lines to all recurrent points.

$$LAM = \frac{\sum_{v=v_{min}}^{N} vP(v)}{\sum_{i,j}^{N} vP(v)} \tag{10}$$

where ***P(v)*** is the probability distribution of the lengths of the vertical lines and v_{min} is the least considered line length.

9. **Trapping time (TT):** is the average length of vertical lines, which is analogous to L for the diagonal lines. TT reflects the average time for a system to stay in a specific state.

$$TT = \frac{\sum_{v=v_{min}}^{N} vP(v)}{\sum_{v=v_{min}}^{N} P(v)} \tag{11}$$

10. **Maximal length of vertical lines (V_{max}):** measures the maximum time that a system holds an unchangeable pattern**.**

$$V_{max} = \max\left(\{v_i\}_{i=1}^{N_v}\right) \tag{11}$$

where N_v is the total number of vertical lines.

11. **Longest length of white vertical line (Rt_{max}):** which is also known as the maximal recurrence time as it implies maximum duration for system to remain in a recurrent state. Higher Rt_{max} values indicate systems that are more predictable.

$$Rt_{max} = \max\left(\{w_i\}_{i=1}^{N_w}\right) \tag{12}$$

where w and N_w are the length and total number of white vertical lines, respectively.

12. **Recurrence time of second type (RT_2):** measures the average value of recurrence time as follows:

$$RT_2 = \frac{1}{N} \sum_{i=1}^{N} T_i^{(2)} \tag{14}$$

where $T_i^{(2)}$ indicates the time of occurrence of the i^{th} recurrence point which is equivalent to the distance between the beginnings of subsequent recurrence structures in RP.

13. **Recurrence period density entropy (RPDE):** reflects the periodicity characteristics of a signal within a dynamical system through the following equation:

$$RPDE = -(\ln T_{max})^{-1} \sum_{t=1}^{T_{max}} P(t) \ln P(t) \tag{15}$$

where T_{max} is the largest recurrence period and ***P(t)*** is the probability distribution of the recurrence time.

14. **Clustering coefficient (Clust):** quantifies how often recurrent states occur as part of small groups that frequently recur together. High clustering coefficients indicate that the recurrent states are strongly interconnected and often occur together, suggesting repetitive dynamics in the system.

$$Clust = \sum_{i=1}^{N} \frac{\sum_{j,k=1}^{N} A_{i,j} A_{j,k} A_{k,i}}{\sum_{j=1}^{N} A_{i,j}} \quad (16)$$

where A is the adjacency matrix and k is the value of each possible neighboring node.

15. **Transitivity (Trans):** is global measure of the interconnectedness in a network. Transitivity measures the likelihood that if two nodes are both connected to a common third node, they are also connected to each other. This provides a sense of the overall clustering in the network.

$$Trans = \sum_{i=1}^{N} \frac{\sum_{j,k=1}^{N} A_{ij} A_{jk} A_{ik}}{\sum_{i,j,k=1}^{N} A_{ij} A_{ik}} \quad (17)$$

RQA features have been successfully implemented for several neurological disease diagnosis using EEG signals. However, RQA features have not yet been properly investigated for AD diagnosis, where only the recurrence rate was previously considered in one of the very early works [18]. In this work, we investigate the usefulness of RQA features for AD diagnosis. Initially, all fifteen RQA features were considered in order to compare their performance to the more commonly implemented Hjorth, statistical, and relative power features. Next, feature ranking will be utilized to identify the most relevant of the RQA features.

3.1.2 Hjorth Parameters

Hjorth parameters are statistical features that can measure signal characteristics related to its complexity [36]. They are widely used for AD detection and were repeatedly shown to improve performance [22], [37]. The details of the three Hjorth parameters are as follows:

1. **Activity**: represents the signal mean power calculated as the variance of the signal. High activity indicates rapid changes in the signal, while low activity indicates a more stable signal.

$$Activity = Var\,(y(t)) \quad (18)$$

2. **Mobility**: describes the signal's mean frequency calculated by finding the square root of the ratio between the variance of the first derivative of the signal and the variance of the signal itself, where the first derivative represents the rate of change of the considered signal. Mobility reflects the amount of change in the signal over time.

$$Mobility = \sqrt{\frac{Var\,(\frac{dy(t)}{dt})}{Var\,(y(t))}} \quad (19)$$

3. **Complexity**: represents changes in signal frequency through calculating the ratio between the mobility of the slope of the signal to the mobility of the signal. Complexity provides a measure of the irregularity of the signal.

$$Complexity = \frac{Mobility\,(\frac{dy(t)}{dt})}{Mobility\,(y(t))} \quad (20)$$

3.1.3 Statistical Features

Statistical features are widely used for AD detection as they have the advantage of being simple while effectively capturing variations in EEG signals. Eight statistical features were implemented in the present work whose details are summarized in Table 3.

Table 3: Statistical features.

Feature	Equation	
Mean (μ)	$\mu = \frac{1}{N}\sum_{i=1}^{N} x_i$	(21)
Variance (σ^2)	$\sigma 2 = \frac{1}{N-1}\sum_{i=1}^{N} \lvert x_i - \mu \rvert^2$	(22)
Standard deviation (σ)	$\sigma = \sqrt{\frac{1}{N-1}\sum_{i=1}^{N} \lvert x_i - \mu \rvert^2} = \sqrt{\sigma 2}$	(23)
Interquartile Range (IQR)	$\mathrm{IQR} = Q3 - Q1$ *where Q3 is the 75th percentile and Q1 is the 25th percentile.*	(24)
Energy (E)	$\mathrm{E} = \sum_{i=1}^{N} \lvert x_i \rvert^2$	(25)
Root Mean Square (RMS)	$\mathrm{RMS} = \sqrt{\frac{1}{N}\sum_{i=1}^{N} \lvert x_i \rvert^2}$	(26)
Kurtosis (K)	$k = \frac{1}{N}\sum_{i=1}^{N} \frac{(x_i - \mu)^4}{\sigma^4}$	(27)
Skewness (S)	$S = \frac{1}{N}\sum_{i=1}^{N} \frac{(x_i - \mu)^3}{\sigma^3}$	(28)

3.1.3 Relative Power (RP)

Power spectral density (PSD) is typically calculated from the signal's FFT to describe its power across different frequency components [38]. PSD features are commonly implemented in EEG studies as they facilitate the analysis of brain electrical activity in the frequency domain. EEG signals can be decomposed into five different frequency bands: delta (δ), theta (θ), alpha (α), beta (β), and gamma (γ). Each band is associated with different states of consciousness and cognitive functions [39]. PSD features capture changes in the specific frequency bands due to AD such as power increase in low frequency bands and power decrease of higher frequency bands [40]. PSD can be calculated using the following equation:

$$P = \frac{\sum_{i=1}^{S} PSD(K_i)}{S} \quad (29)$$

where $\boldsymbol{i}$ is the number of points per epoch, $\boldsymbol{S}$ is the epoch length, $\boldsymbol{K_i}$ is the corresponding FFT coefficient for each point within the epoch.

In the present study, the relative power (RP) of each frequency band divided by the PSD of the whole spectrum is considered for AD diagnosis.

3.2 Classification

SVM is one of the most widely used classifiers in machine learning. In this study, SVM classifier with radial basis function (rbf) kernel was used as it has been previously shown to give reliable results for AD diagnosis. Hyperparameter tuning was performed using a grid search approach in order to find the optimal cost and gamma parameters for the computed EEG features. Both parameters were varied from 10^3 to 10^{-3}, decreasing by a factor of 10 at each step. Accordingly, a cost value of 1000 and gamma value of 0.1 were applied in all experiments.

LOSO CV was implemented in order to assess how well the proposed model generalizes across different individuals. In LOSO, the dataset is divided by subject rather than by instance. Accordingly, training is performed on data from all but one subject and testing is carried out on the excluded unseen subject. This process is repeated N times, N being the number of subjects within the dataset. LOSO simulates practical scenarios making it a more realistic and robust evaluation method for EEG-based models. Nevertheless, 10-fold CV results are also included in this work for comparison with other 10-fold CV experiments reported in literature.

3.3 Performance Metrics

Three performance metrics were considered in this work for the evaluation of the proposed AD diagnosis model which are accuracy, sensitivity, and specificity.

$$Accuracy = \frac{TP + TN}{TP + TN + FP + FN} \tag{30}$$

$$Sensitivity = \frac{TP}{TP + FN} \tag{31}$$

$$Specificity = \frac{TN}{TN + FP} \tag{32}$$

where TP, TN, FP, and FN are the true positive, true negative, false positive, and false negative values, respectively.

4 Results

The aim of this study is to compare RQA features to the several widely implemented features for AD diagnosis which are Hjorth parameters, statistical features, and relative power. All features were computed from 19 EEG channels spanning the different brain regions in order to determine the most relevant brain region for AD vs. HS classification. First, the four considered feature groups were compared considering all the EEG channels considering both LOSO and 10-fold CV experiments. Next, feature ranking was performed to identify the relevant features among the best performing feature group. Finally, the presented method is compared to several other approaches from literature considering the same EEG dataset.

MATLAB R2023b was used for all feature extractions and LOSO CV classification experiments. For the RQA features, a dedicated toolbox for complex systems (TOCSY) was considered that can be found at Ref. [41]. Weka 3.8.6 [42] was utilized for the 10-fold CV experiments, as well as for the feature ranking performed within the final analysis.

4.1 Dataset

In the present study, a public EEG dataset consisting of 36 AD and 29 HS [25] was utilized. For each subject, 19 channels were recorded based on the international 10/20 placement system which are: Fp1, Fp2, F3, F4, Fz, F7, F8, C3, C4, Cz, P3, P4, Pz, O1, O2, T3, T4, T5, and T6. Recording time lasted an average of 13.5 minutes (5.1min → 21.3min) for AD patients and 13.8 minutes (12.5min → 16.5min) for HS. All recordings were acquired at resting state with subject eye closed at a sampling frequency of 500 Hz. All recordings were preprocessed using a Butterworth band-pass filter having a frequency range of 0.5 Hz to 45 Hz. Several artifact rejection methods were applied to eliminate eye and jaws artifacts. In this work, the EEG signals were segmented into 10 second non-overlapping epochs to overcome data scarcity as previously performed in Refs. [18], [43].

4.2 Experimental Results

Figure 4 summarizes the classification accuracies for the SVM classifier with rbf kernel using LOSO CV. For the different features groups, Hjorth and statistical features resulted in accuracies ranging from 40% to 68%. Relative power results were slightly higher with accuracies ranging from 62% to 75%. For the Hjorth, statistical, and relative power features, parietal, occipital, and temporal regions resulted in better performance than the frontal and central regions. Specifically, the highest accuracies attained by Hjorth, statistical, and RP features were 67.5% (O), 56.9% (T), and 74.6% (T), respectively.

Interestingly, RQA features resulted in significantly superior performance compared to the three other considered feature groups with accuracies ranging from 89.6% to 98.0%. The highest RQA accuracy was attained from the central brain region at 98.0%, followed by the frontal and temporal regions at 93.6% and 90.2%, respectively. RQA features are thus shown to outperform the three other feature groups by 25% to 40% indicating their potential for integration within computer-aided AD diagnostic tools. In addition, these superior results were attained considering only three EEG channels which are C3, C4, and Cz. Using a limited number of EEG channels for feature calculations has several merits such as simplified hardware setup and reduced computation complexity.

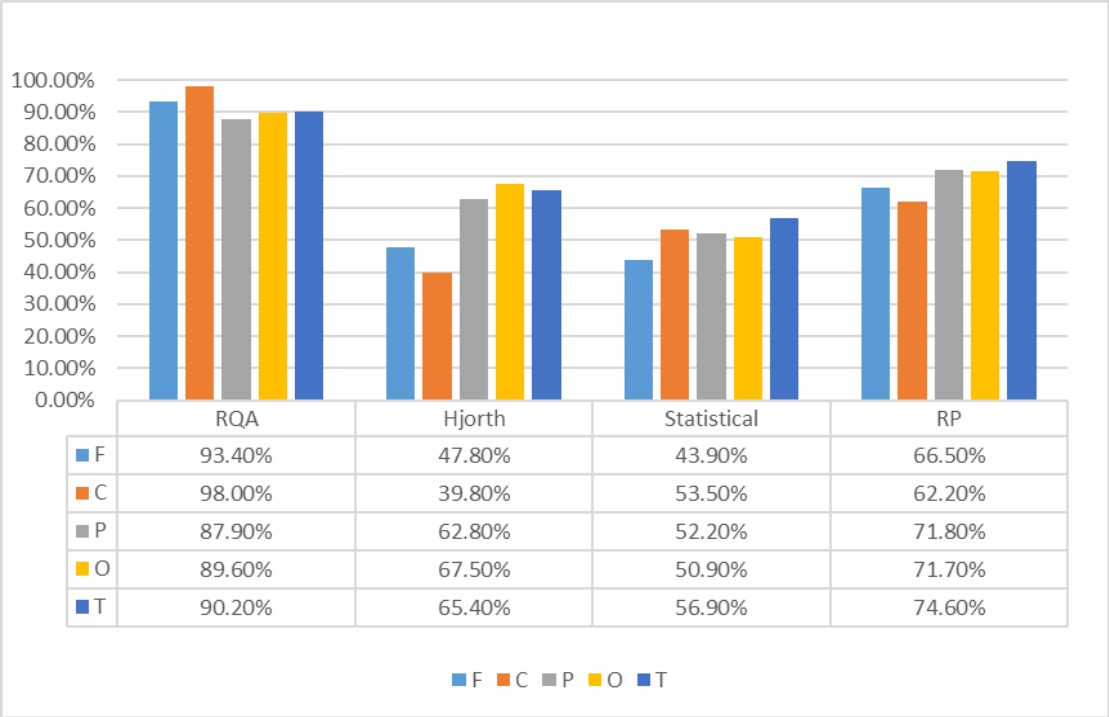

	RQA	Hjorth	Statistical	RP
F	93.40%	47.80%	43.90%	66.50%
C	98.00%	39.80%	53.50%	62.20%
P	87.90%	62.80%	52.20%	71.80%
O	89.60%	67.50%	50.90%	71.70%
T	90.20%	65.40%	56.90%	74.60%

Figure 4. AD diagnosis classification accuracies for the different brain regions considering the four different features groups (RQA – Hjorth – Statistical – Relative Power) using LOSO CV.

Both LOSO and k-fold CV were implemented in literature to asssure the generalization capability of the AD diagnosis methods. LOSO is, however, better suited for subject-specific EEG studies such as for AD diagnosis as it assures that the train and test datasets do not have samples from the same subject. LOSO thus provides a more realistic assessment of the model's ability to work on unseen individuals, which is often the main objective in clinical applications. In this work, we give the results for both LOSO and 10-fold CV.

Tables 4 summarize the AD vs. HS classification results for RQA features computed from the different brain regions considering LOSO CV. RQA features computed from the central brain region are shown to outperform, not only features computed from the other brain regions, but also the features integrated from all the brain regions. For the central RQA features, further analysis was performed to investigate the effect of hyperparameter tuning on performance. Experimental results summarized in Table 5 indicate that performance remained robust regardless of the considered hyperparameter values, where in all cases accuracies remained $\geq$ 92.0%. Additionally, a high sensitivity ($\geq$ 95.0%) was achieved in all cases. For AD diagnosis, a high sensitivity is critically important as it

ensures individuals with the disease are correctly identified to immediately receive the necessary treatment. For the central RQA features, the best performance was achieved with a cost value of 100 and a gamma value of 0.1, resulting in an accuracy of 98.2%, sensitivity of 99.8%, and specificity of 96.3%.

Table 4: AD vs. HS classification performance using RQA features for the different brain regions (LOSO).

	Accuracy	**Sensitivity**	**Specificity**
Frontal (F)	93.4%	93.1%	93.8%
Central (C)	**98.0%**	**99.6%**	**96.0%**
Parietal (P)	87.9%	86.1%	90.2%
Occipital (O)	89.6%	88.4%	91.0%
Temporal (T)	90.2%	88.7%	91.9%
FCPOT	97.1%	98.8%	94.9%

Table 5: AD vs. HS classification performance using central RQA features for different cost and gamma values (LOSO CV).

Cost	**Gamma**	**Accuracy**	**Sensitivity**	**Specificity**
1000	10	92.4%	96.3%	87.7%
	1	94.6%	95.0%	94.2%
	0.1	98.0%	99.6%	96.0%
100	10	92.4%	96.3%	87.7%
	1	96.7%	97.8%	95.4%
	0.1	**98.2%**	**99.8%**	**96.3%**
10	10	92.4%	96.1%	87.9%
	1	97.6%	99.3%	95.5%
	0.1	98.0%	99.8%	95.9%
1	10	93.5%	98.7%	87.2%
	1	97.6%	99.2%	95.5%
	0.1	97.1%	98.7%	95.0%

Table 6 shows the AD vs. HS classification results for RQA features computed from the different brain regions considering 10-fold CV. RQA features computed from the frontal or central regions are shown to give the highest accuracies (98.4%) closely followed by the temporal region (97.5%). Additionally, considering the 19 EEG channels spanning the five different brain regions resulted in an accuracy of 99.8%. Although LOSO CV results are more robust as they indicate the ability of the algorithm to generalize to unseen data, 10-fold CV results are also presented in this work as they are commonly implemented in literature for AD diagnosis using EEG signals. However, k-fold classification results are considered overoptimized since the train and test datasets include instances from the same subjects.

Table 6: AD vs. HS classification performance using RQA features for the different brain regions (10-fold CV).

	Accuracy	Sensitivity	Specificity
Frontal (F)	98.4%	98.4%	98.2%
Central (C)	98.4%	98.4%	98.2%
Parietal (P)	94.6%	94.6%	94.8%
Occipital (O)	95.7%	95.7%	95.8%
Temporal (T)	97.5%	97.5%	97.5%
FCPOT	99.8%	99.8%	99.8%

A recent work by Fouad et al. [44] computed several statistical wavelet-based features from 19-EEG channels for AD diagnosis. In their work, they compared several traditional classifiers including Naïve Bayes (NB), kNN, and SVM to the ResNet50 deep network. Experiments were also performed to compare the relevance of computing the features from the different brain regions. Similar to the analysis in the present study, their results indicated that central region features were associated with the highest accuracies. For the NB classifier, their method resulted in an accuracy of 96.55%, sensitivity of 94.55%, and specificity of 96.29%. For the ResNet50, the same features arranged in a 2D plot results in an accuracy of 97.83%, sensitivity of 98.26%, and specificity of 97.84%. Their results are in general comparable to the results presented in the current study, although the proposed method tended to give better sensitives. However, their results were derived based on the division of their dataset to 40% training and 60% testing as opposed to using LOSO CV which might have led to overoptimized performance and does not assure the generalizability of their approach. In this work, LOSO CV was implemented to assure training and testing datasets do not have samples from the same subject. Experiments showed that considering the RQA features computed from the central brain region resulted in an accuracy of 98.2%, sensitivity of 99.8%, and specificity of 96.3% indicating their effectiveness for AD diagnosis.

In order to investigate the relevance of the fifteen different RQA features calculated from the central brain region, feature ranking was performed using the ReliefF [45] algorithm. ReliefF works by first identifying nearest neighbours for each instance within the dataset. Next, the relevance of each feature is determined based on how well it distinguishes the instance from its nearest neighbours that are from a different class [46]. In the present study, ReliefF was utilized for feature ranking then the lowest relevant features were recursively removed from the feature set. Subsequently, classification was repeated to examine the effect of eliminating this feature on performance. These steps were repeated as long as the classification performance remained the same. Based on this experiment, the seven most relevant RQA features computed from the central brain region were identified to be (1) average diagonal length, (2) recurrence rate, (3) transitivity, (4) entropy, (5) trapping time, (6) determinism, and (7) the ratio between determinism and recurrence rate.

RQA features were previously implemented by Mona et al. [15] for emotion detection from EEG signals. In their work, eleven RQA features were computed resulting in reliable performance that outperformed several other methods from literature. For AD diagnosis, RQA features were scarcely implemented. Among the few works that did use them, Timothy et al. [18] calculated the recurrence rate (RR) from the RQA and CRQA for complexity and synchrony assessment, resulting in accuracies of 72.2% and 80.6%, respectively. Another work by Nunez et al. [43] implemented the TREND RQA feature to study EEG dynamics for AD patients. Although they found statistically significant differences in TREND between HS and AD patients, they did not implement any classification experiments. In this work, fifteen RQA features were computed from the different brain regions and compared to several commonly used feature types from AD diagnosis. RQA were shown to achieve significantly higher performance then all other feature groups regardless of the EEG channel's associated brain region. These results thus highlight the relevance of RQA features for AD diagnosis from EEG signals. Additionally, the high sensitivity achieved by the RQA features is favourable for AD diagnosis as it ensures all subjects with AD are correctly identified. This makes RQA features a reliable tool for early AD detection, minimizing the risk of false negatives in clinical settings.

4.3 Comparison to Previous Methods

Table 7 compares results from the proposed AD diagnosis relying on RQA features, to several other methods from literature considering the same EEG dataset. Previous works commonly considered all EEG channels for feature computations. Among the previous literature, Talaat et. al. [47] achieved the highest performance by combining RQA and statistical features computed from the parietal, occipital, and temporal brain regions reporting an accuracy, sensitivity, specificity of 96.7%, 97.2%, and 96.1%, respectively. Zheng et al. [26] also achieved high performance by integrating spectral, complexity, and synchronization features, attaining an accuracy of 95.86%, a sensitivity of 96.41%, and a specificity of 97.40%. In this work, RQA features from only the three central region channels resulted in an accuracy of 98.2% by that outperforming the different methods from literature by ~ 2-20%. Furthermore, the presented method resulted in a sensitivity of 99.8% which is favourable for reliable AD diagnosis. High sensitivity ensures that the maximum number of AD patients are correctly identified, by that minimizing the chances of misdiagnosis in clinical settings.

EEG devices are highly complicated and bulky mainly being operated by expert technicians within a controlled lab setting [48]. Portable EEG devices are becoming increasingly popular as they can be easily used to monitor brain activity for long periods in unmonitored, out of the lab settings. These recording could then be automatically analysed for primarily diagnosis or disease monitoring of subject patients using computer-aided diagnostic tools. Several portable AD diagnostic methods have already been implemented in literature [49], [50]. Although these methods have shown significant capability to distinguish between AD patients and healthy subject, their performance remains somewhat limited. The proposed method presents an AD diagnostic method that achieves reliable performance using seven RQA features computed from only three central EEG channels (C3, C4 and Cz). RQA features thus have the potential to increase the reliability of computer-aided portable and lab-based AD diagnostic tools.

Table 7. Comparison to previous methods from literature using the same dataset (LOSO).

Paper	Year	EEG Channels	Features	Classifier	Accuracy
Miltiadous et al. [24]	2021	All	RP	RF	77.01%
Miltiadous et al. [25]	2023	All	RP Coherence	CNN & Transformer	83.28%
Zheng et al. [26]	2023	All	Spatial Spectral	RF	95.86%
Talaat et al. [47]	2024	POT	RQA & Statistical	SVM	96.70%
Proposed Model	**2024**	**All** **Central**	**RQA**	**SVM**	**97.10%** **98.20%**

5 Conclusions

Recurrence quantification analysis (RQA) is a non-linear approach used to thoroughly analyze EEG signals. Fifteen RQA features were computed in this work for AD diagnosis. RQA features were compared to three widely implemented feature groups: Statistical - Hjorth - Relative Power. All features were computed from the frontal, central, parietal, occipital, and temporal brain regions. Experiments showed that the RQA features significantly outperformed all other feature groups by 25% to 40%. For all brain regions, the RQA features resulted in accuracies that exceeded 89%. RQA features calculated from the central EEG channels (C3, C4 and Cz) gave the highest performance with an accuracy of 98.2%, sensitivity of 99.8%, and specificity of 96.3% for LOSO CV. Feature ranking was performed using the ReliefF algorithm, resulting in eliminating eight RQA features while maintaining the same performance. The high sensitivity attained by the RQA features is crucial as it ensures individuals with the disease are correctly identified in order to immediately receive the necessary treatment. Additionally, the presented AD diagnosis method considers features computed from solely three EEG channels, making it suitable for portable EEG devices.

Although RQA features were previously implemented in several domains such as emotion detection, autism diagnosis, and epilepsy identification, RQA features have scarcely been utilized for AD diagnosis. Experiments performed in this work show that RQA features are superior to the three other considered feature groups that are widely used for AD diagnosis. RQA features outperformed all other feature groups regardless of the brain region from which they were computed. This work thus sheds light on the potential of RQA features for reliable AD diagnosis, paving the way for further exploration of their applicability in other neurological diagnostic tasks. Future work includes exploring the effectiveness of RQA features in differentiating between mild, moderate, and severe AD, as well as in distinguishing AD from other neurological conditions such as frontotemporal dementia (FTD).

References

[1] Who Health Organization (WHO), "Dementia." Accessed: Sep. 21, 2024. [Online]. Available: https://www.who.int/news-room/fact-sheets/detail/dementia

[2] M. G. Ulep, S. K. Saraon, and S. McLea, "Alzheimer Disease," The Journal for Nurse Practitioners, vol. 14, no. 3, pp. 129–135, 2018, doi: 10.1016/j.nurpra.2017.10.014

[3] "2024 Alzheimer's disease facts and figures," Alzheimer's & Dementia, vol. 20, no. 5, pp. 3708–3821, May 2024, doi: 10.1002/alz.13809

[4] N. Garg, M. S. Choudhry, and R. M. Bodade, "A review on Alzheimer's disease classification from normal controls and mild cognitive impairment using structural MR images," J Neurosci Methods, vol. 384, p. 109745, 2023, doi: 10.1016/j.jneumeth.2022.109745

[5] S. Afzal et al., "Alzheimer disease detection techniques and methods: a review," 2021.

[6] K. AlSharabi, Y. Bin Salamah, A. M. Abdurraqeeb, M. Aljalal, and F. A. Alturki, "EEG Signal Processing for Alzheimer's Disorders Using Discrete Wavelet Transform and Machine Learning Approaches," IEEE Access, vol. 10, pp. 89781–89797, 2022, doi: 10.1109/ACCESS.2022.3198988

[7] A. Modir, S. Shamekhi, and P. Ghaderyan, "A systematic review and methodological analysis of EEG-based biomarkers of Alzheimer's disease," Measurement, vol. 220, p. 113274, 2023, doi: 10.1016/j.measurement.2023.113274

[8] J. H. Kim, C. M. Kim, and M.-S. Yim, "An Investigation of Insider Threat Mitigation Based on EEG Signal Classification," Sensors, vol. 20, no. 21, 2020, doi: 10.3390/s20216365

[9] Mayo Clinic, "How Your Brain Works." Accessed: Oct. 27, 2024. [Online]. Available: https://www.mayoclinic.org/diseases-conditions/epilepsy/in-depth/brain/art-20546821

[10] Olivia Guy-Evans, "Parts of the Brain: Anatomy, Structure & Functions." Accessed: Sep. 21, 2024. [Online]. Available: https://www.simplypsychology.org/anatomy-of-the-brain.html

[11] R. Grujičić, "Central Sulcus." Accessed: Oct. 27, 2024. [Online]. Available: https://www.kenhub.com/en/library/anatomy/central-sulcus

[12] "What Happens to the Brain in Alzheimer's Disease?," National Institute of Aging. Accessed: Sep. 29, 2024. [Online]. Available: https://www.nia.nih.gov/health/alzheimers-causes-and-risk-factors/what-happens-brain-alzheimers-disease

[13] N. Houmani et al., "Diagnosis of Alzheimer's disease with Electroencephalography in a differential framework," PLoS One, vol. 13, no. 3, pp. e0193607–e0193607, Mar. 2018, doi: 10.1371/journal.pone.0193607

[14] A. Horvath, A. Szucs, G. Csukly, A. Sakovics, G. Stefanics, and A. Kamondi, "EEG and ERP biomarkers of Alzheimer's disease: a critical review," FBL, vol. 23, no. 2, pp. 183–220, 2018, doi: 10.2741/4587

[15] M. Elamir, W. Alatabany, and M. Aldosoky, "Intelligent emotion recognition system using recurrence quantification analysis (RQA)," in 2018 35th National Radio Science Conference (NRSC), 2018, pp. 205–213. doi: 10.1109/NRSC.2018.8354365

[16] T. Heunis et al., "Recurrence quantification analysis of resting state EEG signals in autism spectrum disorder – a systematic methodological exploration of technical and demographic confounders in the search for biomarkers," BMC Med, vol. 16, no. 1, p. 101, 2018, doi: 10.1186/s12916-018-1086-7

[17] I. Gruszczyńska, R. Mosdorf, P. Sobaniec, M. Żochowska-Sobaniec, and M. Borowska, "Epilepsy identification based on EEG signal using RQA method," Adv Med Sci, vol. 64, no. 1, pp. 58–64, 2019, doi: 10.1016/j.advms.2018.08.003

[18] L. T. Timothy, B. M. Krishna, and U. Nair, "Classification of mild cognitive impairment EEG using combined recurrence and cross recurrence quantification analysis," International Journal of Psychophysiology, vol. 120, pp. 86–95, 2017, doi: 10.1016/j.ijpsycho.2017.07.006

[19] C. I. Ledesma-Ramírez, J. J. Hernández-Gloria, E. Bojorges-Valdez, O. Yanez-Suarez, and O. Piña-Ramírez, "Recurrence quantification analysis during a mental calculation task," Chaos: An Interdisciplinary Journal of Nonlinear Science, vol. 33, no. 6, p. 063154, Jun. 2023, doi: 10.1063/5.0147321

[20] L. Abdel-Hamid, "An Efficient Machine Learning-Based Emotional Valence Recognition Approach Towards Wearable EEG," Sensors, vol. 23, no. 3, 2023, doi: 10.3390/s23031255

[21] N. S. Amer and S. B. Belhaouari, "EEG Signal Processing for Medical Diagnosis, Healthcare, and Monitoring: A Comprehensive Review," IEEE Access, vol. 11, pp. 143116–143142, 2023, doi: 10.1109/ACCESS.2023.3341419

[22] M. S. Safi and S. M. M. Safi, "Early detection of Alzheimer's disease from EEG signals using Hjorth parameters," Biomed Signal Process Control, vol. 65, p. 102338, 2021, doi: 10.1016/j.bspc.2020.102338

[23] K. D. Tzimourta et al., "EEG Window Length Evaluation for the Detection of Alzheimer's Disease over Different Brain Regions," Brain Sci, vol. 9, no. 4, p. 81, Apr. 2019, doi: 10.3390/brainsci9040081

[24] A. Miltiadous et al., "Alzheimer's Disease and Frontotemporal Dementia: A Robust Classification Method of EEG Signals and a Comparison of Validation Methods," Diagnostics (Basel), vol. 11, no. 8, p. 1437, Aug. 2021, doi: 10.3390/diagnostics11081437

[25] A. Miltiadous et al., "A Dataset of Scalp EEG Recordings of Alzheimer's Disease, Frontotemporal Dementia and Healthy Subjects from Routine EEG," Data (Basel), vol. 8, no. 6, p. 95, 2023, doi: 10.3390/data8060095

[26] X. Zheng et al., "Diagnosis of Alzheimer's disease via resting-state EEG: integration of spectrum, complexity, and synchronization signal features," Front Aging Neurosci, vol. 15, p. 1288295, Nov. 2023, doi: 10.3389/fnagi.2023.1288295

[27] T. Zhou, X. Chen, Y. Shen, M. Nieuwoudt, C.-M. Pun, and S. Wang, "Generative AI Enables EEG Data Augmentation for Alzheimer's Disease Detection Via Diffusion Model," in 2023 IEEE International Symposium on Product Compliance Engineering - Asia (ISPCE-ASIA), 2023, pp. 1–6. doi: 10.1109/ISPCE-ASIA60405.2023.10365931

[28] N. S. Amer and S. B. Belhaouari, "Exploring new horizons in neuroscience disease detection through innovative visual signal analysis," Sci Rep, vol. 14, no. 1, p. 4217, Feb. 2024, doi: 10.1038/s41598-024-54416-y

[29] J.-P. Eckmann, S. O. Kamphorst, and D. Ruelle, "Recurrence plots of dynamical systems," World Scientific Series on Nonlinear Science Series A, vol. 16, pp. 441–446, 1995, doi: 10.1142/9789812833709_0030

[30] N. Marwan and C. L. Webber, "Mathematical and Computational Foundations of Recurrence Quantifications," in Recurrence Quantification Analysis: Theory and Best Practices, Jr. Webber Charles L. and N. Marwan, Eds., Cham: Springer International Publishing, 2015, pp. 3–43. doi: 10.1007/978-3-319-07155-8_1

[31] N. Marwan, M. Carmen Romano, M. Thiel, and J. Kurths, "Recurrence plots for the analysis of complex systems," Phys Rep, vol. 438, no. 5, pp. 237–329, 2007, doi: 10.1016/j.physrep.2006.11.001

[32] E. J. Ngamga, S. Bialonski, N. Marwan, J. Kurths, C. Geier, and K. Lehnertz, "Evaluation of selected recurrence measures in discriminating pre-ictal and inter-ictal periods from epileptic EEG data," Phys Lett A, vol. 380, no. 16, pp. 1419–1425, 2016, doi: 10.1016/j.physleta.2016.02.024

[33] N. Marwan, J. F. Donges, Y. Zou, R. V Donner, and J. Kurths, "Complex network approach for recurrence analysis of time series," Phys Lett A, vol. 373, no. 46, pp. 4246–4254, 2009, doi: 10.1016/j.physleta.2009.09.042

[34] S. Martín-González, J. L. Navarro-Mesa, G. Juliá-Serdá, G. M. Ramírez-Ávila, and A. G. Ravelo-García, "Improving the understanding of sleep apnea characterization using Recurrence Quantification Analysis by defining overall acceptable values for the dimensionality of the system, the delay, and the distance threshold," PLoS One, vol. 13, no. 4, pp. e0194462-, Apr. 2018, [Online]. Available: 10.1371/journal.pone.0194462

[35] S. P. Arunachalam, S. Kapa, S. K. Mulpuru, P. A. Friedman, and E. G. Tolkacheva, "Rotor pivot point identification using recurrence period density entropy," Biomed Sci Instrum, 2017, doi: 10.1109/EMBSISC.2016.7508597

[36] B. Hjorth, "EEG analysis based on time domain properties," Electroencephalogr Clin Neurophysiol, vol. 29, no. 3, pp. 306–310, 1970, doi: 10.1016/0013-4694(70)90143-4

[37] S. Hadiyoso, T. L. E. R. Mengko, and H. Zakaria, "Complexity Analysis of EEG Signal in Patients with Cognitive Impairment Using the Hjorth Descriptor," in 2019 2nd International Conference on Bioinformatics, Biotechnology and Biomedical Engineering (BioMIC) - Bioinformatics and Biomedical Engineering, 2019, pp. 1–5. doi: 10.1109/BioMIC48413.2019.9034794

[38] J. Dempster, "CHAPTER SIX - Signal Analysis and Measurement," in The Laboratory Computer, J. Dempster, Ed., London: Academic Press, 2001, pp. 136–171. doi: 10.1016/B978-012209551-1/50039-8

[39] P. A. Abhang, B. W. Gawali, and S. C. Mehrotra, "Chapter 2 - Technological Basics of EEG Recording and Operation of Apparatus," in Introduction to EEG- and Speech-Based Emotion Recognition, P. A. Abhang, B. W. Gawali, and S. C. Mehrotra, Eds., Academic Press, 2016, pp. 19–50. doi: 10.1016/B978-0-12-804490-2.00002-6

[40] J. Jeong, "EEG dynamics in patients with Alzheimer's disease," Clinical Neurophysiology, vol. 115, no. 7, pp. 1490–1505, 2004, doi: 10.1016/j.clinph.2004.01.001

[41] "Recurrence Plot & Quantification." Accessed: Sep. 27, 2024. [Online]. Available: https://tocsy.pik-potsdam.de/rp.php

[42] I. H. Witten, E. Frank, M. A. Hall, and C. J. Pal, Data Mining, Fourth Edition: Practical Machine Learning Tools and Techniques, 4th ed. San Francisco, CA, USA: Morgan Kaufmann Publishers Inc., 2016.

[43] P. Núñez et al., "Characterization of EEG Resting-state Activity in Alzheimer's Disease by Means of Recurrence Plot Analyses," in 2019 41st Annual International Conference of the IEEE Engineering in Medicine and Biology Society (EMBC), 2019, pp. 5786–5789. doi: 10.1109/EMBC.2019.8856600

[44] I. A. Fouad and F. El-Zahraa M. Labib, "Identification of Alzheimer's disease from central lobe EEG signals utilizing machine learning and residual neural network," Biomed Signal Process Control, vol. 86, p. 105266, 2023, doi: 10.1016/j.bspc.2023.105266

[45] I. Kononenko, "Estimating attributes: Analysis and extensions of RELIEF," in Machine Learning: ECML-94, F. Bergadano and L. De Raedt, Eds., Berlin, Heidelberg: Springer Berlin Heidelberg, 1994, pp. 171–182, doi: 10.1007/3-540-57868-4_57

[46] R. J. Urbanowicz, M. Meeker, W. La Cava, R. S. Olson, and J. H. Moore, "Relief-based feature selection: Introduction and review," J Biomed Inform, vol. 85, pp. 189–203, 2018, doi: 10.1016/j.jbi.2018.07.014

[47] M. Talaat, M. Awadalla, and L. Abdel-Hamid, "Alzheimer's Disease Diagnosis using EEG Signals: Investigating Complexity, Time and Spectral Features," in ICBSP '24: Proceedings of the 2024 9th International Conference on Biomedical Imaging, Signal Processing, ACM, 2024, p. 129-136.

[48] A. J. Casson, "Wearable EEG and beyond," Biomed Eng Lett, vol. 9, no. 1, pp. 53–71, 2019, doi: 10.1007/s13534-018-00093-6

[49] M. Hata et al., "Utilizing portable electroencephalography to screen for pathology of Alzheimer's disease: a methodological advancement in diagnosis of neurodegenerative diseases," Front Psychiatry, vol. 15, p. 1392158, 2024, 10.3389/fpsyt.2024.1392158

[50] L. Pu, K. M. Lion, M. Todorovic, and W. Moyle, "Portable EEG monitoring for older adults with dementia and chronic pain - A feasibility study," Geriatr Nurs (Minneap), vol. 42, no. 1, pp. 124–128, 2021, doi: 10.1016/j.gerinurse.2020.12.008